An analytic model for Tropical cyclone outer winds

Timothy W. Cronin[1]

[1]Program in Atmospheres, Ocean, and Climate, MIT, Cambridge, Massachusetts, USA

Key Points:

- Analytic solutions are derived for the previously unsolved outer wind model of Emanuel (2004).
- Analytic wind profile calculations enable faster merged wind profile calculations, following Chavas et al. (2015).
- Scaling of merged wind profiles suggests decreases in the radius of maximum wind with warming, at constant outer size.

Corresponding author: Timothy Cronin, `twcronin@mit.edu`

Abstract

The variation of Tropical cyclone azimuthal wind speed (V) with distance from storm center (r) is a fundamental aspect of storm structure that has important implications for risk and damages. The theoretical model of Emanuel (2004), which applies well outside the rainy core of the storm, matches radiatively-driven subsidence and Ekman suction rates at the top of the boundary layer to obtain a nonlinear differential equation for dV/dr. This model is particularly appealing because of its strong physical foundation, but has no known analytic solution for $V(r)$. In this paper, I obtain an analytic solution to $V(r)$ for the Emanuel (2004) outer wind model. Following previous work, I then use this solution to explore properties of merged wind models that combine the outer model with an inner model that applies to the rainy core of a storm.

Plain Language Summary

The swirling winds of hurricanes extend far away from their centers, fading away into background weather. Previous work has proposed a theoretical model to explain how these swirling winds decrease with distance from the storm center for areas outside the rainy core of the storm. But this model has not previously been solved with pencil-and-paper methods. I find a new mathematical formula that solves the model for how winds weaken away from the center of a hurricane. I then use the solutions to examine how hurricane winds near the center of a storm relate to the winds far from the center, and what this implies about how hurricanes behave.

1 Introduction

The swirling or azimuthal winds (V) of a Tropical cyclone increase rapidly away from its calm eye to a maximum in the eyewall, then decrease much more gradually with radius (r), fading away into the background flow. This radial profile of swirling winds – which I will refer to as the "wind structure," "wind profile," or simply $V(r)$ – encapsulates important relationships among variables in a Tropical cyclone, including the maximum swirling wind speed, V_m, the radius at which these maximum winds are attained, r_m, and the far outer radius of the storm where the winds vanish, r_0. These all can influence the destructive capability of a storm, with outer size of a storm particularly important for storm surge damage (e.g., Powell & Reinhold, 2007; Irish & Resio, 2010; Lin & Chavas, 2012). For real storms, r_0 is difficult to measure directly and requires azimuthal averaging in any nonzero background flow, so Tropical cyclone size is commonly quantified using the radius of a certain fixed value of wind speed (e.g., gale-force winds) or the radius of a closed surface pressure contour, instead of the radius of vanishing winds (e.g., Frank, 1977; Merrill, 1984; Chavas & Emanuel, 2010). Numerous empirical models of wind structure have been developed and are widely used; for example, the elegant work of Holland (1980) fits the observed dependence of pressure on radius using a logarithmic rectangular hyperbola, with gradient wind balance then enabling calculation of $V(r)$. Empirical wind structure models, however, cannot identify the dynamical or kinematic constraints that might bound or link intensity, radius of maximum winds, and outer size, or provide insight on how $V(r)$ might change in a warming climate. Emanuel (2004) and Emanuel and Rotunno (2011) developed physics-based models of, respectively, storm outer and inner structure: these two were cleverly merged into a complete theoretical wind model by Chavas et al. (2015) (See schematic of merged winds in Figure 1). The inner wind model of Emanuel and Rotunno (2011) assumes a slantwise-moist-neutral core of the storm, where the radial gradients in wind speed outside the eyewall are constrained by wind shear and mixing in the outflow, and has known analytic solutions (in the limit of a cyclostrophic vortex). The outer wind model of Emanuel (2004) is based on the (sound) assumption that subsidence due to radiative cooling matches Ekman suction at the top of the boundary layer in the outer region of the storm where there is little rain and deep

61 convection. This outer wind model, however, has been formulated only as a nonlinear
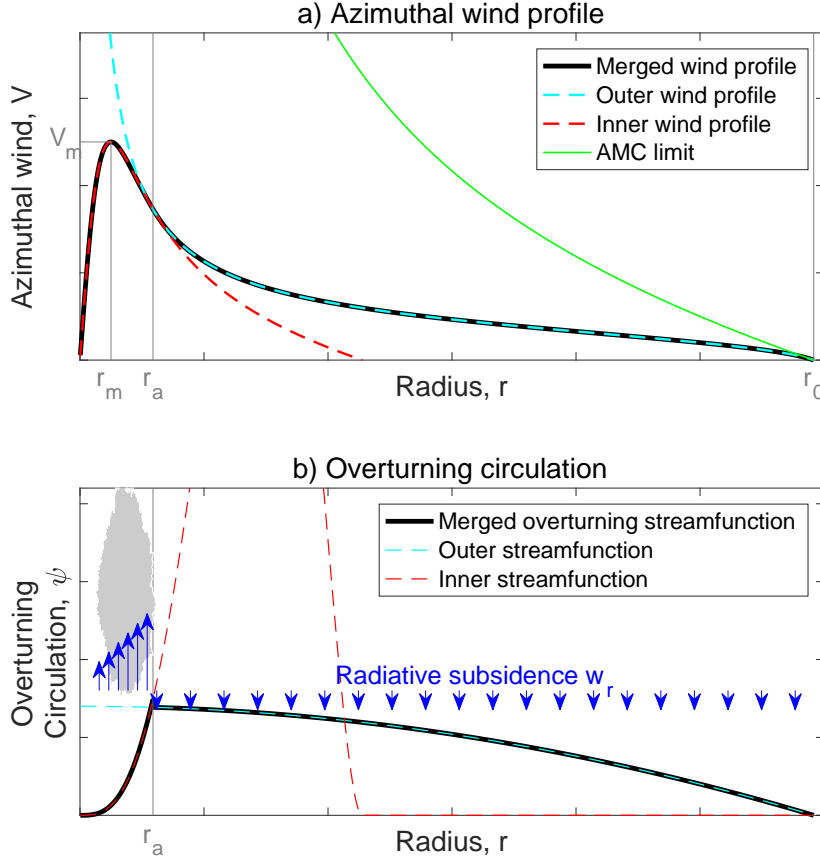62 differential equation for dV/dr, and lacks a known analytic solution for $V(r)$.

a) Azimuthal wind profile

Figure 1. a) Azimuthal or swirling winds, V, of a Tropical cyclone plotted against radius, r. General features include the radius of maximum wind, r_m, the maximum wind speed V_m, and the radius of vanishing wind, r_0. The specific profile drawn in black merges the Emanuel (2004) outer wind model (cyan dashed line) and the Emanuel and Rotunno (2011) inner wind model (red dashed line), following Chavas et al. (2015). The theoretical angular-momentum-conserving wind profile (green), and the merge radius r_a are also drawn. b) The overturning circulation in the radius-height plane generally includes ascent at small radii, and sinking at large radii. Merged wind profiles of Chavas et al. (2015) have a continuous overturning streamfunction (ψ) at r_a, but a discontinuity in vertical velocity, and assume a constant radiative-subsidence speed w_r for $r > r_a$.

63   This paper has two main goals. The first is to derive an analytic solution for the
64 outer wind structure model of Emanuel (2004) (Section 2), and apply this solution to
65 accelerate the calculation of merged wind profiles (Section 3), using the merger approach
66 of Chavas et al. (2015). This work may be of broad interest: the outer wind profile model
67 of Emanuel (2004) is a major theoretical accomplishment that has remained under-appreciated,
68 likely due to the lack of known closed-form solutions. The code provided as part of this
69 work (Cronin, 2023) may also be of broad interest to researchers who model hurricane

risk, as it accelerates such wind profile calculations by a factor of ~ 50, relative to the code of Chavas (2022).

The second goal is to leverage these solutions to consider how $V(r)$ may be constrained in present or future climates. I find that in the part of parameter space corresponding to real-world cyclones, merged profiles follow a scaling close to $c_D r_m V_m^2 f^{-1} \sim w_r r_0^2$, where f is the Coriolis parameter, c_D the drag coefficient, and w_r the radiative-subsidence speed (Section 4). This scaling can be justified by considering the total ascent and descent associated with the overturning circulation, and it indicates that in a future climate, storms with the same outer size will likely have a smaller radius of maximum winds due to both increases in V_m and decreases in w_r. Findings here do not rely on the analytic solution to the outer wind profile, but this section is facilitated by both faster solutions to merged profiles and also by prior discussion of the inner and outer wind solutions. Finally, I close with a summary of findings, and some thoughts about limitations and future directions (Section 5).

2 Derivation

Emanuel (2004) derives an expression for the radial gradient of the azimuthal wind (dV/dr) outside the rainy core of a Tropical cyclone, based on the angular momentum budget of the boundary-layer inflow. In steady state at a given radius, the absolute angular momentum averaged over the boundary layer depth, $M = rV + \frac{1}{2}fr^2$, is increased by inward radial advection of air with higher M, and decreased by torque due to surface stress, $c_D V^2$. Taking ψ as the cyclone's overturning circulation streamfunction in the radius-height plane at the top of the boundary layer (vertical velocity $w = \frac{1}{r}\frac{d\psi}{dr}$), this balance is:

$$\psi \frac{dM}{dr} = c_D r^2 V^2. \tag{1}$$

In the outer regions of the storm, where there are no convective updrafts, ψ must increase with decreasing radius to accommodate sinking air at the top of the boundary layer. This air is thermodynamically constrained to descend at the radiative-subsidence speed $w_r = \dot{Q}/\frac{d\theta}{dz}$, where $\dot{Q}$ is the radiative cooling rate of air just above the top of the boundary layer, and θ is the potential temperature (using the convention $w_r > 0$ for subsidence). Over Tropical oceans, radiative-subsidence speeds are typically on the order of millimeters per second, and the drag coefficient $c_D \sim 10^{-3}$. If the circulation of the storm vanishes at some outer radius, r_0, the streamfunction at $r < r_0$ can be directly obtained by integrating w_r over the annulus between r and r_0: $\psi(r) = w_r(r_0^2 - r^2)/2$ (e.g., Figure 1). This balance can equivalently be viewed as requiring a match between the Ekman suction rate at the top of the boundary layer,

$$w_{\text{Ek}} = \frac{1}{r}\frac{d}{dr}\left(\frac{rc_D V^2}{f+\zeta}\right), \tag{2}$$

and the radiative-subsidence velocity, because the absolute vorticity $f+\zeta$ in the denominator of the Ekman suction can be written as $\frac{1}{r}\frac{dM}{dr}$. Either view leads to the same conclusion: the absolute angular momentum in the non-convective outer portion of the storm increases with radius according to:

$$\frac{dM}{dr} = \frac{2c_D(rV)^2}{w_r(r_0^2 - r^2)}, \tag{3}$$

which gives the following equation for V:

$$\frac{d(rV)}{dr} = \frac{2c_D(rV)^2}{w_r(r_0^2 - r^2)} - fr. \tag{4}$$

This is a Riccati equation with no known closed-form solution, but it can be transformed into a second-order ODE by a change of variables. I show below that this transformed

equation is amenable to a quickly-converging power series solution when expanded in a coordinate $x \equiv 1 - r/r_0$ that varies from 0 at the outer edge of the storm to 1 at storm center.

Using primes to denote derivatives of a function q with respect to r, a general Riccati equation of the form:

$$q' = A(r)q^2 + B(r) \tag{5}$$

can be rewritten as a second-order homogeneous ODE in a transformed function y, where $qA(r) = -y'/y$:

$$A(r)y'' - A'(r)y' + [A(r)]^2 B(r)y = 0. \tag{6}$$

Applying this result to Equation 4 with $q = rV$ and simplifying slightly gives:

$$(r_0^2 - r^2)y'' - 2ry' - 2\frac{c_D f}{w_r}ry = 0. \tag{7}$$

If a solution for $y(r)$ can be found, then V is given by $\frac{2c_D r V}{w_r(r_0^2 - r^2)} = \frac{-y'}{y}$. I factor V into two terms:

$$V = \underbrace{\left\{\frac{f(r_0^2 - r^2)}{2r}\right\}}_{V_{AMC}(r)} \underbrace{\left[-\frac{w_r}{c_D f}\frac{y'}{y}\right]}_{G(r)}, \tag{8}$$

where the first term (in braces), labeled $V_{AMC}(r)$, is the angular-momentum-conserving azimuthal wind speed for inflow from a quiescent state at radius r_0 inward to radius r. The second term (in brackets), labeled $G(r)$, is the fractional reduction of wind speed relative to V_{AMC} due to loss of angular momentum by surface friction. Physical solutions for $G(r) \equiv -\frac{w_r}{c_D f}[y'/y]$ must be bounded on $[0, 1]$, and the appropriate boundary condition is $G(r) = 1$ at $r = r_0$. Note that since y'/y has dimensions of inverse distance, w_r distance per time, f inverse time, and c_D is dimensionless, $G(r)$ is also dimensionless.

Equation 7 can be solved with a power series in r, but this series converges slowly and has an undetermined free parameter that does not clearly relate to the outer boundary condition ($G(r) = 1$ at $r = r_0$). However, a change of variables in equation 7, to:

$$x \equiv 1 - r/r_0, \tag{9}$$

gives a power series solution that both converges comparatively quickly and easily matches the outer boundary condition. Since $dx = -dr/r_0$, Equation 7 expressed in terms of x (with an $_{(x)}$ subscript on a primed term denoting a derivative with respect to x) becomes:

$$x(2 - x)y''_{(x)} + 2(1 - x)y'_{(x)} - 2\gamma(1 - x)y = 0, \tag{10}$$

where $\gamma \equiv c_D f r_0 w_r^{-1}$ is identical to the nondimensional outer wind parameter found in Chavas and Lin (2016). Note that the solution for G is expressed in terms of $y' = dy/dr = (dy/dx)(dx/dr) = -(1/r_0)y'_{(x)}$, so $G(r) = \frac{w_r}{c_D f r_0}[y'_{(x)}/y] = \gamma^{-1}[y'_{(x)}/y]$.

The power series solution to Equation 10, given by $y = \sum_{n=0}^{\infty} a_n x^n$, can be taken generally to have $a_0 = 1$ (the choice of a_0 does not affect G since it does not alter the ratio $y'_{(x)}/y$), leading to the first few terms and recurrence relation for coefficients as follows:

$$
\begin{aligned}
a_1 &= \gamma \\
a_2 &= \frac{\gamma^2}{(2!)^2} \\
a_3 &= \frac{\gamma^2(\gamma - 1)}{(3!)^2} \\
a_n &= \frac{1}{n^2}\left\{[\gamma + n(n-1)/2]a_{n-1}\right\} - \frac{1}{n^2(n-1)^2}\left\{[\gamma(n-1)^2]a_{n-2}\right\} \qquad [n > 2]. (11)
\end{aligned}
$$

143 (Here, terms outside braces that are factored out show that one can write a_n as $1/(n!)^2$
144 multiplied by a degree-n polynomial in γ with integer coefficients – a fact used further
145 in Text S1.) The power series of the derivative $y'_{(x)}$, is given by $y'_{(x)} = \sum_{n=0}^{\infty}(n+1)a_{n+1}x^n$,
146 so:

$$
\begin{aligned}
G(r) = \frac{y'_{(x)}/\gamma}{y} \quad &= \quad \frac{\sum_{n=0}^{\infty}\frac{a_{n+1}}{\gamma}(n+1)x^n}{\sum_{n=0}^{\infty}a_n x^n} \\
&= \quad \frac{1 + \frac{\gamma}{2}x + \frac{\gamma(\gamma-1)}{12}x^2 + ...}{1 + \gamma x + \frac{\gamma^2}{4}x^2 + \frac{\gamma^2(\gamma-1)}{36}x^3 + ...}.
\end{aligned} \tag{12}
$$

147 The last line here also shows that since $x = 0$ at $r = r_0$ this expression satisfies the
148 outer boundary condition of $G(r) = 1$ at $r = r_0$.

149   The wind speed relative to the angular-momentum-conserving limit, $G(r)$, is a func-
150 tion of the parameter $\gamma \equiv c_D f r_0 / w_r$. $G(r)$ decreases slowly with decreasing radius for
151 small γ, and strongly with decreasing radius, particularly near $r = r_0$, for larger val-
152 ues of γ (Figure 2a). A larger outer radius, drag coefficient, or Coriolis parameter all cor-
153 respond to a greater torque on the inflow and a greater reduction in angular momentum,
154 whereas a larger radiative-subsidence speed leads to stronger radial advection of angu-
155 lar momentum by a stronger overturning circulation, and thus a weaker dependence of
156 G on r. Real-world storms typically have $\gamma \sim 10-100$. No more than a few dozen terms
157 in the series for the numerator and denominator of G are required to attain very small
158 errors in the solution, with the required number of terms increasing with increasing γ
159 (Figure 2b). Errors are benchmarked against a power series solution that uses 100 terms
160 in each of the numerator and denominator. This result suggests that series solutions should
161 be relatively efficient for calculating outer wind profiles, though more computationally
162 efficient methods may exist. Further details of results including numerical implementa-
163 tion of vectorized calculation of $G(r)$ and approximate solutions to $G(r)$ are presented
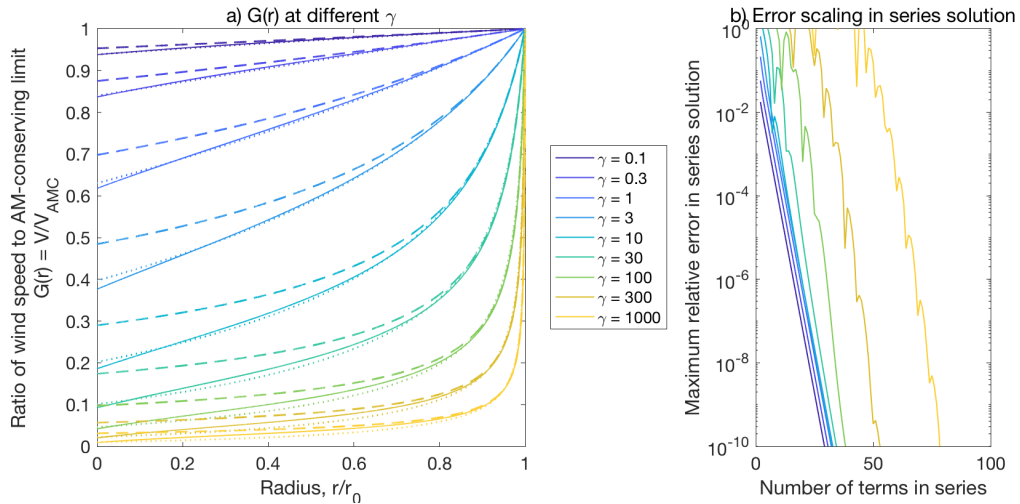164 in Text S1 and Text S2, respectively.

Figure 2. a) Relative azimuthal wind speed $G(r) = V(r)/V_{\text{AMC}}(r)$, as a function of r/r_0, for several values of $\gamma = c_D f r_0 / w_r$ (solid). Also shown are Bessel function (G_b, dashed) and empirical (G_e, dotted) approximations (Text S2). b) Dependence of maximum relative error (over $0 < r < r_0$) with the number of terms in the power series.

3 Merging with the inner wind profile

Chavas et al. (2015) merge solutions for the outer wind profile of Emanuel (2004) and the convective core wind profile of Emanuel and Rotunno (2011). I follow the same procedure, whereby V and dV/dr are matched for inner and outer profiles, but with analytic outer wind profiles in hand.

I consider the maximum azimuthal wind speed V_m and the radius of maximum winds r_m as known variables, and the merge radius between inner and outer profiles r_a and the outer radius r_0 as unknowns (r_a and r_0 are generally shown as normalized by r_m). For a ratio of enthalpy exchange to drag coefficients $c_k/c_D = 1$, the inner wind profile from Emanuel and Rotunno (2011) (their Equation 36) becomes:

$$\frac{V_{\text{in}}}{V_x} = \frac{(r/r_x)}{2(V_x/fr_x)(1+(r/r_x)^2)} \left[(4(V_x/fr_x)+1) - (r/r_x)^2 \right], \tag{13}$$

where $V_x \approx V_m$ and $r_x \approx r_m$. It is (unfortunately) necessary to draw a distinction between the speed V_x and radius r_x used in this expression and the "true" values of V_m and r_m, because these two are not generally identical. Equation 13 does not generally have $\max(V_{\text{in}}) = V_x$ at $r = r_x$; instead this limit applies only when $V_x/(fr_x) >> 1$. The true radius of maximum winds for Equation 13, r_m, is about 5% inward of r_x when $V_x/(fr_x) = 10$, and about 0.5% inward of r_x when $V_x/(fr_x) = 100$. Correcting for this difference is necessary to get a reasonable match to previous results (Chavas, 2022) and so that the input values of V_m and r_m and the outputs from my code match. As part of the solution, several iterations are used to solve for the values of r_x and V_x in Equation 13 that give $\max(V_{\text{in}}) = V_m$ at $r = r_m$.

Taking V_m and r_m as known parameters, two dimensionless variables that govern merged solutions are:

$$\tilde{w}_Q = \frac{w_r}{c_D V_m} \tag{14}$$

$$\text{Ro} = \frac{V_m}{fr_m}, \tag{15}$$

where $\tilde{w}_Q$ is a normalized radiative-subsidence speed (following Emanuel, 2004; Chavas & Emanuel, 2014) that represents a ratio of the outer descent rate to the Ekman pumping ascent in the center of the storm, and Ro is the inner-core Rossby number. Although the outer wind profile has been solved analytically (Equation 12), analytic solution for the merge radius r_a and outer radius r_0 as a function of Ro and $\tilde{w}_Q$ remains infeasible. Instead, numerical solution is used: for a given (Ro, w_Q) pair, the inner wind profile is specified and the outer wind profile depends on the to-be-determined value of r_0. An iterative loop scans through several choices of r_0 to find a value that gives an outer wind profile tangent to the inner wind profile at a single point: the merge radius r_a. This follows a similar approach to Chavas and Lin (2016), but they search through slightly different variables.

The normalized outer radius r_0/r_m increases with decreasing $\tilde{w}_Q$ and increasing Ro, while the normalized merge radius r_a/r_m increases with increasing $\tilde{w}_Q$ and increasing Ro (Figure 3). The outer wind parameter, $\gamma = c_D fr_0 w_r^{-1} = (r_0/r_m)\tilde{w}_Q^{-1}\text{Ro}^{-1}$, thus increases with decreasing $\tilde{w}_Q$ and Ro – unsurprising from its definition – but indicating that r_0/r_m increases sub-linearly with Ro in this parameter range. For sufficiently large $\tilde{w}_Q$, particularly at small Ro, there is no merge point and no outer wind regime at all: the inner wind profile of Emanuel and Rotunno (2011) extends to the edge of the storm (sections shaded gray in Figure 3). This matches the finding of Cronin and Chavas (2019) that wind profiles for dry hurricanes have little contribution from the outer wind regime. In Text S3, I use analytic outer wind solutions to derive an approximate bound on this subset of parameter space, and find that it corresponds roughly to the inequal-

209 ity:

$$\tilde{w_Q} \geq \tilde{w_Q}^* = \frac{16 \mathrm{Ro}^{1/2}}{27}. \tag{16}$$

210 The dotted line in Figure 3 shows that this approximation generally succeeds in delim-
211 iting the part of parameter space without an outer-wind component to the merged pro-
212 files, particularly at lower Ro.

213 The rough position of real tropical cyclones in this joint $(\tilde{w_Q}, \mathrm{Ro})$ parameter space
214 in Figure 3 is indicated by colored dots for representative median storms of different in-
215 tensity categories, using data from Figure 10 of Chavas et al. (2015). Colors of light gray,
216 dark gray, green, yellow, orange, and red, respectively, indicate low-intensity Tropical Storms,
217 high-intensity Tropical Storms, Category 1 Hurricanes, Category 2 Hurricanes, Category
218 3 Hurricanes, and Category 4/5 Hurricanes. Fixed values of $c_D = 0.001$ and $w_r = 0.002$
219 m s^{-1} are used in plotting these points. As in Chavas et al. (2015), the ratio r_0/r_m –
220 of outer size to the radius of maximum winds – increases strongly with intensity, the nor-
221 malized merge radius r_a/r_m increases weakly with intensity, and (not discussed previ-
222 ously) $\gamma \approx 15 - 20$ is strikingly similar across representative storms from different in-
223 tensity classes. Because $\gamma = c_D f r_0/w_r$ – and f, c_D, and w_r all vary comparatively lit-
224 tle with storm intensity – the relative constancy of γ with storm intensity is consistent
225 with the known weak correlation between intensity and storm outer radius (e.g., Chavas
226 & Emanuel, 2010).

227 Further details of methods and results for how merged wind profile calculations are
228 performed and benchmarked against previous code (Figure S1) are presented in Text S4.
229 By using the analytic outer wind profiles described above, together with vectorized cal-
230 culations of multiple wind profiles at once and use of lookup tables for key variables (Text
231 S1, S4), acceleration by about a factor of ~ 50 is obtained relative to the code of Chavas
232 (2022), with comparable or greater accuracy. This corresponds to a computation time
233 of about 10^{-4} to 10^{-3} seconds per wind profile on a single core of a laptop computer when
234 many (> 100) profiles are computed at a time.

4 Discussion and scaling of merged profiles

236 In the region of parameter space characteristic of present-day Tropical cyclones ($5 <$
237 $\mathrm{Ro} < 50$ and $0.02 < \tilde{w_Q} < 0.2$; see Figure 3), an approximate power-law fit for merged
238 solutions is given by $r_0/r_m \sim \mathrm{Ro}^{0.5} \tilde{w_Q}^{-0.5}$. These powers are approximate and the power
239 of Ro slightly smaller than 0.5, but this form is used because a clean approximate scal-
240 ing relationship results from it among V_m, r_m, and r_0:

$$r_0 \sim r_m^{0.5} V_m f^{-0.5} c_D^{0.5} w_r^{-0.5}. \tag{17}$$

241 How to consider this relationship depends on which storm parameters one views as ex-
242 ternally constrained, and which others one thus seeks to predict. In a diagnostic sense,
243 this scaling seems promising in terms of ability to explain and in some cases reconcile
244 seemingly disparate dependences of r_0 on sea-surface temperature, rotation rate, and sur-
245 face moisture availability (Khairoutdinov & Emanuel, 2013; Zhou et al., 2014; Cronin
246 & Chavas, 2019). Recent work on cyclone outer size, however, suggests taking the per-
247 spective that r_0, V_m, c_D, f, and w_r may all be viewed as externally constrained under
248 future climate change (e.g., Chavas & Reed, 2019). Rearranging this expression as a scal-
249 ing relationship for the radius of maximum winds then implies that r_m will likely decrease
250 with warming for storms with the same outer size, the same or greater intensity, and in
251 similar latitude bands. Before discussing this implication, however, it is useful to try to
252 gain a physical understanding of Equation 17.

253 The wind merger condition that V and dV/dr be continuous also implies that the
254 inner and outer streamfunctions must match at the merge radius. Equation 17 can be

rearranged to emphasize this constraint that the upward mass transport in the inner region (left-hand side) must match the downward mass transport in the outer region (right-hand side):

$$c_D r_m V_m^2 f^{-1} \sim w_r r_0^2. \tag{18}$$

Note that I will use "mass transport" as a stand-in for the more accurate term "volume transport" here – reasonable if imperfect when referring to transport across the top of a cyclone's boundary layer at different radii where density may vary by $\sim 10\%$ (the two are also implicitly equated in Emanuel, 2004). It is comparatively straightforward that the downward mass transport can be written as $w_r r_0^2$, because constant subsidence has been assumed over the annulus between r_a and r_0, and $(r_0^2 - r_a^2) \approx r_0^2$ if $r_0 \gg r_a$. But why does the upward mass transport scale as $c_D r_m V_m^2 f^{-1}$? If r_a/r_m were constant, then the inner part of the storm would have upward mass transport that scaled with inner-core Ekman pumping rate, or $c_D V_m r_m^2$ (e.g., Khairoutdinov & Emanuel, 2013), yet this scaling differs slightly. Rearranging Equation 1 shows that that the overturning stream-function can be calculated if V and M are known:

$$\psi = \frac{c_D r^2 V^2}{dM/dr}. \tag{19}$$

In Text S5 I find that this allows the integrated mass transport for the inner wind profile (Equation 13) to be approximated as:

$$\psi(r_a) = c_D V_m r_m^2 \left(\frac{r_a}{r_m} \right)^3. \tag{20}$$

If r_a/r_m depends primarily on Ro, as seen near the colored dots in Figure 3, then this may be subject to further simplification. If $r_a/r_m \sim \mathrm{Ro}^{1/3}$, then the approximate form in Equation 18 is recovered exactly. Thus, Equations 17 and 18 emerge from a combination of mass continuity, and the dependence of r_a/r_m on $\tilde{w}_Q$ and Ro – particularly the gradual increase of r_a/r_m with Ro. I know of no theoretical basis for any specific dependence of r_a/r_m on Ro, so this result highlights the importance of examining total cyclone upward mass transport in both real and simulated storms in future study. With this physical interpretation established, I consider application of Equation 18 to the question of how storm structure may change with climate warming.

Specifically, I will consider how r_m may change with warming at fixed r_0. A bit of explanation is warranted regarding this null hypothesis of constant r_0 with warming, which may surprise some readers (this hypothesis is described and substantiated further by Schenkel et al., 2023). Past studies have found mixed results regarding changes in outer size with climate warming, partly due to use of different metrics of size, and partly due to different idealizations across simulations. Simulations of cyclones on an $f-$plane often (though not universally) show an outer size that is bounded above by V_p/f (e.g., Chavas & Emanuel, 2014, where V_p is the potential intensity) – a length scale that increases with climate warming due to increasing V_p. An upper limiting "potential size" with similar scaling has also recently been given more theoretical rigor (Wang et al., 2022). The outer size of real-world cyclones, however, increases with latitude, directly counter to a $1/f$ scaling (Chavas et al., 2016). Chavas and Reed (2019) hypothesized that a crucial feature missing from $f-$plane simulations is the meridional dependence of f, or beta effect. They used numerical simulations with varied rotation rate and planetary size to show that a vortex Rhines scale $\sim (aV_\beta/(df/d\phi))^{1/2}$, where a is the planetary radius and V_β an outer circulation wind speed, likely limits cyclone size in Earth's Tropics, while a V_p/f bound may apply at higher latitudes. Critically, the vortex Rhines scale is essentially invariant with climate warming. Taken together, these results suggest that cyclones in Tropical latitudes may change little in outer size with climate warming – a result borne out by one idealized study that also shows size increases with warming at higher latitudes (e.g., Stansfield & Reed, 2021).

301   Thus, rearranging Equation 17, if r_0 is treated as a constant, and f also taken as
302 fixed, r_m is expected to decrease with warming due to increasing V_m and decreasing w_r:

$$r_m \sim w_r r_0^2 f V_m^{-2} c_D^{-1}. \tag{21}$$

303   The radiative-subsidence speed w_r is expected to decrease modestly by $\sim 1{-}2\%$ K^{-1}
304 with surface warming due to increases in lower-tropospheric static stability along a moist
305 adiabat. Potential intensity is also expected to increase modestly by $\sim 1{-}2\%$ K^{-1} with
306 surface warming (e.g., Khairoutdinov & Emanuel, 2013; Zhou et al., 2014), with changes
307 in mean actual intensity somewhat more uncertain. Thus, expected changes in V_m and
308 w_r combine to predict a $d\log r_m/dT \sim -5\%$ K^{-1} decrease in radius of maximum winds
309 (at fixed f, r_0, and c_D), although some of this decrease could be offset by a poleward
310 expansion of Tropical cyclone tracks. This leads to the hypothesis that more intense storms
311 may have considerably smaller radii of maximum winds in a warmer climate – a result
312 seen in some modeling studies (Chen et al., 2020; Xi et al., 2023) but worthy of deeper
313 investigation.

5 Conclusions

315   The outer wind model of Emanuel (2004) has finally been analytically solved. So-
316 lutions take the form of a ratio of two power series in a normalized radius variable $x =$
317 $(1{-}r/r_0)$ which varies between 0 at the outer edge of the storm and 1 at the storm cen-
318 ter. The power series converge relatively quickly, and depend on one nondimensional pa-
319 rameter $\gamma = c_D f r_0/w_r$ (as in Chavas & Lin, 2016). The new solution is used to speed
320 up calculations of complete wind models (merging the outer wind model of Emanuel (2004)
321 and the inner wind model of Emanuel and Rotunno (2011) as in Chavas et al. (2015)).
322 For merged solutions, I find that an approximate scaling relationship $r_0 \sim r_m^{0.5} V_m f^{-0.5} c_D^{0.5} w_r^{-0.5}$
323 holds well over the range of parameter space relevant for real Tropical cyclones. This scal-
324 ing is physically consistent with constraints posed by the overturning circulation of a cy-
325 clone, together with a dependence of the size of the ascent region on the inner-core Rossby
326 number $V_m/(f r_m)$ that is an emergent result of matching wind profiles from the two re-
327 gions. If future storms have greater maximum wind speeds and a similar distribution of
328 outer sizes (r_0), then this scaling predicts decreases in maximum wind radii with climate
329 warming: good news.

330   An important result of the paper is that analytic solutions can be used to calcu-
331 late merged wind profiles with considerably less computational cost than the numerical
332 integration of Equation 3 by Chavas (2022). This may make the code developed here (Cronin,
333 2023) immediately useful for risk modeling and assessment. A limitation of the analytic
334 approach, however, is that the drag coefficient, c_D, cannot be allowed to vary with wind
335 speed as in existing numerical solutions (Chavas, 2022).

336   The Emanuel (2004) outer wind model is a major theoretical accomplishment, yet
337 it has not been widely adopted by the community of researchers who study Tropical cy-
338 clones – likely due in part to the lack of a closed-form solution. I hope that the solutions
339 provided here (and the code to implement them) spurs further adoption and testing of
340 the validity of the outer wind model, and perhaps useful approximations of it that are
341 simpler still to implement. A limitation of the outer wind model, especially near r_0, is
342 that its derivation from Equation 1 has assumed a surface torque that scales as $c_D V^2$,
343 where V is the swirling wind of the cyclone. For values of V much smaller than a back-
344 ground wind speed V_0, an azimuthal-mean torque $\sim c_D V_0 V$ would be more appropri-
345 ate; both limits ($V >> V_0$ and $V << V_0$) can be captured by a torque $c_D V \sqrt{V_0^2 + V^2}$.
346 I have not attempted analytic solution of Equation 1 using such a functional form, and
347 the problem does not seem tractable by the Riccati equation solution method used above.

348   An extension of this work that is more analytically tractable, and possibly more
349 useful, is the reduction in bias of the complete wind profiles by adding a third region be-

tween ascending inner and descending outer regions. Chavas et al. (2015) find that real storms deviate most from the profile of the merged model at radii somewhat greater than the merge radius. In this region, observed winds decrease less rapidly with radius than the merged model predicts, and precipitation extends well beyond r_a, violating the assumptions of the outer wind model. Analysis of the overturning circulation above suggests that the jump in assumed behavior at r_a is perhaps even more troubling than realized by Chavas et al. (2015): vertical velocities w_{in} within the inner ascending region are often maximal at r_a; this can be seen by plotting:

$$w_{\mathrm{in}} = \frac{1}{r}\frac{d\psi_{\mathrm{in}}}{dr} = \frac{c_D V_m (r/r_m)}{16\mathrm{Ro}^2\left(1 + \frac{1}{2\mathrm{Ro}}\right)}\left[(4\mathrm{Ro}+1) - (r/r_m)^2\right]\left[3(4\mathrm{Ro}+1) - 7(r/r_m)^2\right]. \quad (22)$$

Chavas et al. (2015) suggest that a natural assumption for an intermediate region would be to take $w = 0$; as a consequence ψ would be constant in the join region between inner ascending and outer descending wind profiles. This assumption replaces $(r_0^2 - r^2)$ in the denominator of Equation 4 with a constant. The resulting equation for V is solvable by the same methods I used above, and the intermediate function y is a solution to the Airy equation ($y'' - ry = 0$). Questions about the utility, uniqueness, and interpretation of such a three-region merged solution for the wind profile are left for future work.

Finally, this study has focused on a steady-state wind profile, in which radial angular momentum advection by the mean overturning circulation balances surface friction. Such a framework does not directly provide any information about how the wind profile behaves in time-evolving situations, including what might drive gradual expansion of the outer radius (e.g., Cocks & Gray, 2002; Chavas & Emanuel, 2010), more rapid changes in inner structure where r_m and V_m vary together, or the important problem of eyewall replacement cycles and secondary eyewall formation. The wind profile model will also fail in regions where other terms are important in the steady angular momentum budget, including vertical advection by the mean circulation, or convergences of eddy angular momentum fluxes in the vertical or horizontal. Nevertheless, particularly given the hypothesis that secondary eyewall formation results from a mismatch or adjustment of the inner core to the outer structure of the storm (Shivamoggi, 2022), a solid understanding of a physics-based steady wind profile seems an important foundation for building further insight into the behavior of Tropical cyclones.

Open Research Section

Acknowledgments

References

Chavas, D. R. (2022, Jun). *Code for tropical cyclone wind profile model of Chavas et al (2015, JAS)*. Retrieved from https://purr.purdue.edu/publications/4066/1 doi: 10.4231/CZ4P-D448

Chavas, D. R., & Emanuel, K. (2014). Equilibrium tropical cyclone size in an idealized state of axisymmetric radiative–convective equilibrium. *Journal of the Atmospheric Sciences*, *71*(5), 1663–1680.

Chavas, D. R., & Emanuel, K. A. (2010). A QuikSCAT climatology of tropical cyclone size. *Geophysical Research Letters*, *37*(18), 10–13.

Chavas, D. R., & Lin, N. (2016). A model for the complete radial structure of the tropical cyclone wind field. Part II: Wind field variability. *Journal of the Atmospheric Sciences*, *73*(8), 3093-3113. doi: 10.1175/JAS-D-15-0185.1

Chavas, D. R., Lin, N., Dong, W., & Lin, Y. (2016). Observed tropical cyclone size revisited. *Journal of Climate*, *29*(8), 2923–2939.

Chavas, D. R., Lin, N., & Emanuel, K. (2015). A model for the complete radial structure of the tropical cyclone wind field. Part I: Comparison with observed structure. *Journal of the Atmospheric Sciences*, *72*(9), 3647–3662.

Chavas, D. R., & Reed, K. (2019). Dynamical aquaplanet experiments with uniform thermal forcing: System dynamics and implications for tropical cyclone genesis and size. *Journal of the Atmospheric Sciences*, *76*, 2257–2274. doi: 10.1175/JAS-D-19-0001.1

Chen, J., Wang, Z., Tam, C.-Y., Lau, N.-C., Dickson Lau, D.-S., & Mok, H.-Y. (2020). Impacts of climate change on Tropical cyclones and induced storm surges in the Pearl River Delta region using pseudo-global-warming method. *Scientific Reports*, 10:1965. doi: 10.1038/s41598-020-58824-8

Cocks, S. B., & Gray, W. M. (2002). Variability of the outer wind profiles of western North Pacific typhoons: Classifications and techniques for analysis and forecasting. *Monthly Weather Review*, *130*(8), 1989–2005.

Cronin, T. W. (2023, Mar). *Code for "An analytic model for Tropical cyclone outer winds"*. Retrieved from https://doi.org/10.5281/zenodo.7783251 doi: 10.5281/zenodo.7783251

Cronin, T. W., & Chavas, D. R. (2019). Dry and semidry tropical cyclones. *Journal of the Atmospheric Sciences*, *76*, 2193–2212. doi: 10.1175/JAS-D-18-0357.1

Emanuel, K. (2004). Tropical cyclone energetics and structure. *Atmospheric turbulence and mesoscale meteorology*(8), 165–191.

Emanuel, K., & Rotunno, R. (2011, 2012/01/04). Self-stratification of tropical cyclone outflow. Part I: Implications for storm structure. *Journal of the Atmospheric Sciences*, *68*(10), 2236–2249.

Frank, W. M. (1977). The structure and energetics of the tropical cyclone. Part I: Storm structure. *Monthly Weather Review*, *105*(9), 1119–1135.

Holland, G. J. (1980). An analytic model of the wind and pressure profiles in hurricanes. *Monthly Weather Review*, *108*(8), 1212–1218.

Irish, J. L., & Resio, D. T. (2010). A hydrodynamics-based surge scale for hurricanes. *Ocean Engineering*, *37*(1), 69–81.

Khairoutdinov, M., & Emanuel, K. (2013). Rotating radiative-convective equilibrium simulated by a cloud-resolving model. *Journal of Advances in Modeling Earth Systems*, *5*(4), 816–825.

Lin, N., & Chavas, D. (2012). On hurricane parametric wind and applications in storm surge modeling. *Journal of Geophysical Research: Atmospheres (1984–2012)*, *117*(D9).

Merrill, R. T. (1984). A comparison of large and small tropical cyclones. *Monthly Weather Review*, *112*(7), 1408–1418.

Powell, M. D., & Reinhold, T. A. (2007). Tropical cyclone destructive potential by integrated kinetic energy. *Bulletin of the American Meteorological Society*, *88*(4), 513–526.

Schenkel, B. A., Chavas, D., Lin, N., Knutson, T., Vecchi, G., & Brammer, A. (2023). North atlantic tropical cyclone outer size and structure remain unchanged by the late twenty-first century. *Journal of Climate*, *36*, 359–382. doi: 10.1175/JCLI-D-22-0066.1

Shivamoggi, R. (2022). *Secondary eyewall formation as a response to evolving tropical cyclone wind structure* (PhD Dissertation). Massachusetts Institute of Technology, Department of Earth, Atmospheric and Planetary Sciences.

Stansfield, A., & Reed, K. (2021). Tropical cyclone precipitation response to surface warming in aquaplanet simulations with uniform thermal forcing. *Journal of Geophysical Research: Atmospheres*, *126*. doi: 10.1029/2021JD035197

Wang, D., Lin, Y., & Chavas, D. R. (2022). Tropical cyclone potential size. *Journal of the Atmospheric Sciences*, *79*, 3001–3025. doi: 10.1175/JAS-D-21-0325.1

Xi, D., Lin, N., & Gori, A. (2023). Increasing sequential tropical cyclone hazards along the US East and Gulf coasts. *Nature Climate Change*, *13*, 259–265. doi: 10.1038/s41558-023-01595-7

Zhou, W., Held, I. M., & Garner, S. T. (2014). Parameter study of Tropical cyclones in rotating radiative–convective equilibrium with column physics and resolution of a 25-km GCM. *Journal of the Atmospheric Sciences*, *71*(3), 1058–1069.

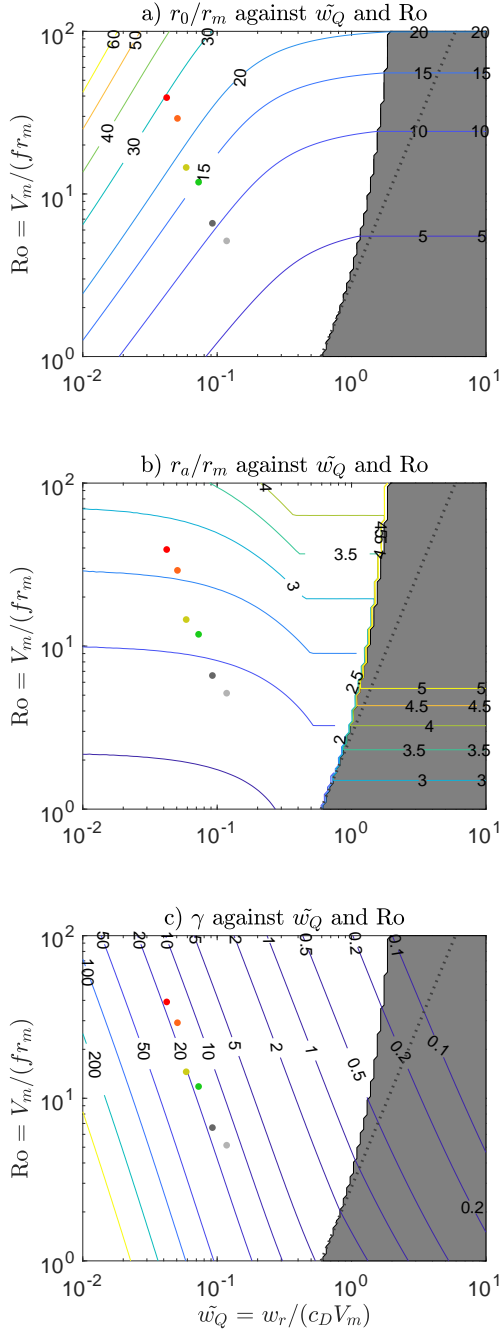**Figure 3.** a) Normalized outer radius, r_0/r_m, for merged solutions as a function of nondimensional radiative-subsidence parameter $\tilde{w}_Q$ and inner core Rossby number Ro. Gray shading indicates the region of parameter space where the no outer wind solution is needed, and the black dotted line shows an approximate bound on this limit (Equation 16). Colored dots represent observed median storms from different intensity categories of Chavas et al. (2015); intensity increases from gray to red (see text for more details). b) Normalized merge radius r_a/r_m: inner solution applies for $r < r_a$ and outer solution for $r > r_a$. c) Outer wind nondimensional parameter γ.